Title
Origin, structure, and role of background EEG activity. Part 4: Neural frame simulation

Journal
Clinical Neurophysiology, 117(3)

ISSN
1388-2457

Author
Freeman, Walter J, III

Publication Date
2006-03-01

Peer reviewed

Origin, structure, and role of background EEG activity
Part 4. Neural frame simulation

Clinical Neurophysiology 117 (3): 572-589

Walter J Freeman
Department of Molecular & Cell Biology
University of California at Berkeley
Berkeley CA 94720-3206 USA
Tel 1-510-6442-4220 fax 1-510 –643-9290
wfreeman@socrates.berkeley.;edu http://sulcus.berkeley.edu

Running title: Neural frame simulation

Key words: Hilbert transform, neural frame, noise (1/f), phase slip, simulated EEG, spatial power spectral density (PSD_X), volume conduction

Acknowledgment
I am grateful to Brian C. Burke for software development. Examples of simulated EEGs will be available for download from the above website.

Abstract

Objective: To develop a method for simulating background EEG based on the premise that the activity from synaptic excitation among populations of neurons can be modeled with the filtered output of a random number generator.
Methods: The logarithm of the amplitude of activity was weighted in accordance with 1/f, the log frequency in both temporal (PSD_T) and spatial (PSD_X) spectra. The activity was spatially smoothed by volume conduction. Further deviation from full randomness was by sustained spatial coherence averaging 25% of total power. The departure from the background state to an active state, as seen in the awake EEG, was simulated by adding segments that were 90% correlated while attenuating by 50% the uncorrelated background activity in those segments. Spatial amplitude modulation was imposed on the correlated noise to create signals that simulated AM patterns.
Results: The statistical properties of the EEG were replicated, including the PSD_T, PSD_X, point spread function (PSF), partitioning of the variance with PCA, and the percentages of correct classification of AM patterns.
Conclusions: The essential change that identified a frame in EEG was transient increase in synchrony among a population of cortical neurons in the beta or gamma band of the PSD_T. The limitation on classification efficacy was imposed by high variance in AM patterns in successive frames with the same artificial spatial pattern.
Significance: This method of simulation provides a test bed with which to develop improved techniques for digital signal processing to extract behaviorally relevant information from the EEG at human-machine interfaces.

1. Introduction

The high spatial resolution achieved for multichannel EEG by high-density electrode arrays on neocortical surfaces in trained animals revealed serial spatial patterns in response to presentation of conditioned stimuli that resembled stationary cinematographic frames [Freeman, 2005]. The EEG patterns in the frames were spatial amplitude modulations (AM) of a spatially coherent, aperiodic oscillatory waveform, which was defined as a carrier wave. The power spectral densities (PSD) of the EEGs had power-law distributions (1/f) in log-log displays; the maximal energy of carrier waves was in spectral peaks in the beta (12-30 Hz) or gamma (30-80 Hz) ranges, while the repetition of frames gave peaks in the theta and alpha ranges [Freeman, Burke and Holmes, 2003]. The onset of each frame was by a state transition in which the phase of the carrier wave was re-initialized and then re-synchronized within a few ms, whereupon its AM pattern emerged, stabilized, increased in intensity to a brief maximum, and then decayed after 3 to 5 cycles of the carrier wave with phase and frequency dispersion [Freeman, 2004a,b]. Replication of the results in Part 3 [Freeman, 2005] is the aim of the present report.

Demonstration of these findings depended heavily though not exclusively on use of the analytic signal expressed in the EEG, which was derived using Hilbert transform giving high temporal resolution of the near-instantaneous phase. However, the Hilbert transform revealed irregular and unpredictable jumps in phase known as “phase slip” [Pikovsky, Rosenblum and Kurths, 2001]. The phase of a nearly periodic oscillation having a peak frequency could be represented as continually increasing, but the presence of a low frequency low frequency baseline shift could occasionally preclude a zero crossings between peaks of the oscillation and therefore cause sudden forward jumps in phase. High frequency components that caused multiple zero crossings between peaks could cause sudden backward jumps in phase. The phase slip from the Hilbert transform of a broadband signal resembled a random walk of unpredictable jumps. Band pass filtering was essential for application of the Hilbert transform to aperiodic signals, but when the pass band was too narrow, the coherent oscillations were distorted and the temporal resolution of phase changes was lost [Le Van Quyen et al., 2001; Quiroga et al. 2002]. Optimization of band pass filters by empirical mode decomposition [Huang et al., 1998] was designed to analyze phase slip, but it lacked sufficient temporal resolution to track repetitive state transitions sought in EEGs. An alternative method for optimization [Freeman, 2004b] was based on calculation of tuning curves to fix high and low pass frequencies, in accordance with the criterion of optimal classification of the AM patterns in the multi-channel EEGs with respect to the conditioned stimuli (CSs) used to induce them.

Justification for using the analytic amplitude and analytic phase was based on a physiological theory of the mechanism of the carrier wave as generated by fields of self-organized neural activity through regenerative (positive) feedback among excitatory cortical neurons, temporally modulated by negative feedback interaction among excitatory and inhibitory neurons, and spatially modulated by positive feedback among inhibitory neurons [Freeman, 1975; 2004a,b]. In most areas the EEG manifested the potential differences established by the flow of dendritic current of the excitatory neurons across the relatively fixed tissue impedance of the cortical tissue (an exception being the olfactory bulb where EEG current was from the inhibitory interneurons). This current controlled the pulse densities comprising outputs of pyramidal cells (or bulbar mitral cells). In rather general conditions of symmetry the output of the inhibitory

neurons lagged the output of excitatory neurons by π/2 radians (90°); therefore the EEG corresponded to the output of the forward limb of the neural negative feedback loop, and its Hilbert transform in quadrature corresponded to the output of the feedback loop (the reverse for the bulb). Treating the EEG as the real part (excitatory) and its Hilbert transform as the imaginary part (inhibitory) gave the analytic signal as a complex number at each digitizing time step. The sum of squares of the real and imaginary parts gave estimates of the instantaneous power required by respectively the excitatory and inhibitory neurons in local areas of cortex for dendritic currents. The square root of that sum gave the analytic amplitude, which proved to give the best available estimate of AM patterns [Freeman, 2004a]. The nonlinear interactions at multiple levels provided the means for modeling conditional stability, instability, and repetitive state transitions by which AM patterns formed. The arctangent of the ratio of the imaginary and real parts gave the analytic phase, which proved to give the best available estimates of the times of state transitions for onset and offset of frames [Freeman, 2004b].

This field theory incorporated elements of related theories of the EEG that postulated its origin in local distributed feedback [Basar, 1998] and in noise: Gaussian [Bullock, 1969; Elul, 1972], 1/f [Linkenkaer-Hansen et al., 2001; Hwa and Ferree, 2002; Wakeling, 2004], and chaotic [Tsuda, 2001; Stam et al., 2003]. Other theories have explained EEG oscillations in terms of thalamocortical interactions [Andersen and Andersson, 1968; Steriade, 1997; Hoppensteadt and Izhkevich, 1998; Miller and Schreiner, 2000]; reaction rates of membrane permeabilities [Traub et al., 1996; Whittington et al., 2000]; interactions of cortical modules each with its characteristic frequency [Kelso, 1995; Houk, 2005], statistical mechanics [Wilson and Cowan, 1973, Ingber, 1995; Friston, 2000]; and resonant modes of wave mechanics [Nunez, 1981]. Mechanisms of sequences of state transitions have been modeled by others in terms of metastability [Kelso, 1995; Friston, 1997; Bressler and Kelso, 2001; Fingelkurts and Fingelkurts, 2004] and chaotic itinerancy [Tsuda, 1961]. Very likely these other components of a more general model play roles in EEG dynamics, but they are not required for present purposes.

Detection of state transitions in EEGs is important in brain studies of cognition, stages of sleep, and mechanisms of loss of stability in seizures [Freeman et al., 2005]. The problem addressed here is how to distinguish physiological state transitions from spurious phase slip, both of which are revealed by the Hilbert transform. The need is for a method first to simulate multiple EEG signals that have the statistical properties known to characterize background EEG but that are stationary (with negligible change in frequency), and second to simulate state transitions at known times so as to evaluate existing methods for avoiding false negative and false positive identifications. This report presents such a method based on cortical anatomy and physiology and describes its advantages and limitations. The chief targets of simulation are the aperiodic oscillatory waveforms of the EEG; its $1/f^2$ temporal PSD_T and spatial PSD_X; its point spread functions (PSF) on the cortical surface; its nearly Gaussian amplitude histograms; its distributions of eigenvalues under PCA (Principal Components Analysis); the power-law distributions of parameters derived from the analytic amplitude and analytic phase by the Hilbert transform; and especially the levels of % correct classification of simulated AM patterns.

The method did not simulate the nonlinear neurodynamics that generated the neural activity seen in the EEG. The neurodynamics of the olfactory EEG has been simulated by constructing a nested hierarchy of model populations (“K-sets”) that have been the main tools with which to

describe local EEG dynamics with differential equations [Freeman, 1975, 2000] or probability distributions derived from random graph theory ("neuropercolation" [Kozma et al., 2004]). The equations were solved to replicate the EEG generated by the populations and to simulate simple cognitive behaviors controlled by the primordial forebrain [Kozma and Freeman, 2001; Kozma, Freeman and Erdí, 2003]. However, the models do serve to specify that the source of the background "spontaneous" neural activity could be conceived as the synaptic interaction of excitatory cortical pyramidal neurons, each neuron transmitting to $\sim 10^4$ neurons and receiving synaptic input from $\sim 10^4$ neurons. The sparseness of cortical connection density meant that each neuron had synapses with <1% of the neurons within its dendritic radius [Braitenberg and Schüz, 1991], but with sufficient interconnection density to transmit more pulses to other neurons than it received from other neurons. In engineering terms each neuron maintained positive feedback with its neighborhood at sufficiently strength to exceed unity gain at least transiently. The mean firing rates were stabilized by refractory periods [Freeman, 2000] that effectively constrained the interaction strengths and supported emergence of a point attractor governing the collective output. In a piece-wise linear approximation to the dynamics the attractor appeared as a real-valued pole at the origin of the complex plane [Freeman, 1975].

The small-signal linearized transfer function for the feedback path conformed to that of a one-dimensional diffusion process, so that the sustained pulse activity for each neuron was randomized on each pass through its neighborhood. The pulse train transmitted by each neuron was low-pass filtered through its dendrites that acted in accordance with the cable equation and summed over the neurons in the neighborhood. The resulting EEG had nearly Gaussian amplitude histograms [Elul, 1972; Freeman, 1975] and Poisson-like properties of the pulse trains of individual neurons [Freeman, 2000]. These properties could not be explained by integrate-and-fire neuron models; the conclusion was reached that the background activity was an emergent property of the neighborhood, which was manifested in aperiodic individual pulse trains and steady-state pulse densities of neighborhoods. In the present study this complexity was simplified by representing the output of each neighborhood (a set of 4-6 hypercolumns under a surface electrode) by an i.i.d. random numbers with Gaussian distribution, zero mean and unit standard deviation (SD) as the starting point of the simulation. To simulate an array of spatially uncorrelated EEGs, 64 i.i.d. were generated. A 65^{th} i.i.d. was generated and replicated on 64 channels to simulate spatially correlated EEG activity as seen in carrier waves.

The oscillations in the background EEG depended on the negative feedback relation among excitatory and inhibitory neurons, which necessitated the sustaining excitation provided by the mutually excitatory pyramidal neurons. Symmetry and the high spatial frequencies of textures in AM patterns required mutual inhibition among the inhibitory neurons to provide contrast enhancement, resulting in the robustly stable broad-spectrum oscillations seen in the basal EEG [Freeman, 1975/2004] and the textured AM patterns seen in active states. The spatiotemporal patterns of phase modulation (PM) and the power-law distributions of the parameters by which the PM patterns were described supported the conclusion that the neocortex maintained itself at self-organized criticality [Linkenkaer-Hansen, 2001; Wakeling, 2004; Freeman, 2004b], in which the stabilized critical parameter was the mean firing rate of every cortical neuron, that was maintained by local homeostasis. Those stabilized firing rates were of course subject to up- or down-regulation by neuromodulatory controls of the states of arousal and focused attention in cerebral dynamics [Panksepp, 1998]. A key feature of the simulation was to determine an

optimal set of parameters to yield sustained background EEG, and then repeatedly to provide the simulated sensory input that was required to break the symmetry of the background activity and induce a state transition with formation of a spatial AM pattern.

The simulation using random numbers required (i) temporal filtering to give 1/f amplitude spectra of temporal frequencies; (ii) spatial filtering to give 1/f amplitude spectra of spatial frequencies; (iii) spatial convolution to simulate volume conduction; (iv) a basal level of 25% covariance to simulate the level of background spatial synchrony; (v) higher levels of covariance to simulate frames of increased spatial coherence established in cortex by behaviorally correlated state transitions manifested in the EEG; and (vi) imposition of 4 patterns of arbitrary spatial amplitude modulation of the synchronized random number carrier waves to simulate AM patterns for classification. The aim was to start with the simple model of random numbers having varying levels of spatial coherence, to learn what constraints would be required to simulate AM patterns, and to identify the limitations on the simple model as the basis for conducting more advanced studies of brain dynamics through the EEG.

Significant differences in power spectral properties were found in three states: sleep; awake and at rest; awake and engaged in cognitive behavior. Intelligibility of results required simulations of all three states. Human data were acquired at rest and in deep slow wave sleep with video monitoring (episodes of REM sleep were not identifiable in EEGs from the array placement in this subject); rabbit data were acquired at rest and active. Examples from both sets were included for this presentation of results. Differences between species were matters of scale [Freeman et al., 2005].

2. Methods

The details of laboratory and clinical EEG data acquisition and processing have been published in previous reports on rabbits [Barrie, Freeman and Lenhart, 1996; Freeman, 2004a,b] and the human subject [Freeman et al. 2005]. All computations were done with MATLAB, including those for PSD, PSF, PCA, histograms and the Hilbert transform.

2.1 Temporal processing

The interconnected cortical pyramidal cells in a neighborhood of 4-6 hypercolumns formed the element for simulation, because the limit on spatial resolution of spatial wavelength of the EEG recorded at the pial surface was about 2 mm (Freeman, 1975/2004). Simulation of the background signal of each neighborhood was begun with a random number generator from a single seed to get 64 uncorrelated time series with 1000 values in a Gaussian i.i.d. The numbers were generated at time intervals corresponding to digitizing intervals of 2 ms (rabbit) or 5 ms (human) in epochs 2 s or 5 s in duration. A 65^{th} signal was generated to give 64 copies. Basal EEG in the rest awake state was formed by adding 25% spatially correlated noise and 75% uncorrelated noise. EEG in active awake states was formed by adding 10% uncorrelated noise and 90% correlated noise in short epochs. Each signal was filtered 0.1-100 Hz to simulate the analog pass band of the EEG. The entire 2 s to 5 s of each time series was transformed by the FFT, filtered by equation (1), and transformed back to the time series by the inverse FFT. The 1/f filter had a coefficient, α that determined the slope of the filter in log-log coordinates:

$$V'(f) = - \alpha \text{ antilog}_{10} [V(f)], \quad (1)$$

where f was frequency in Hz, V was the magnitude before filtering, V' was the magnitude after filtering, and $\alpha = 1$. The quality of simulation was checked at each stage by comparing the noise filtered in the desired beta or gamma pass bands (Fig. 1, A) with the EEG (B) recorded in the same way from an awake human subject. The temporal PSD_T of the filtered uncorrelated noise (Fig. 1, C, black curve) conformed to $1/f^2$ as expected. The PSD_T of the EEG (D) had multiple peaks above the $1/f^2$ base that were simulated (C, gray curve) by adding correlated noise to the uncorrelated noise before filtering (see Section 3.2). The $1/f^3$ PSD_T (Fig. 1, F) seen in sleep was simulated (E) by filtering uncorrelated noise using equation (1) with $\alpha = 1.5$ [Freeman et al., 2005].

2.2. Spatial processing

Simulation of spatial properties of EEGs required solutions to three problems: source-sink geometry and locations; point spread functions (PSF) to simulate volume conduction; and filtering to construct 1/f forms of PSD_X from the PSF and EEGs. Distinguishing the characteristics of EEG in states of active awake, rest awake, and sleep required use of both human and animal EEG data. PSDX were calculated with the FFT in two dimensions and averaged on the basis of experimental findings of radial symmetry [Freeman, 2004b; Freeman et al., 2003].

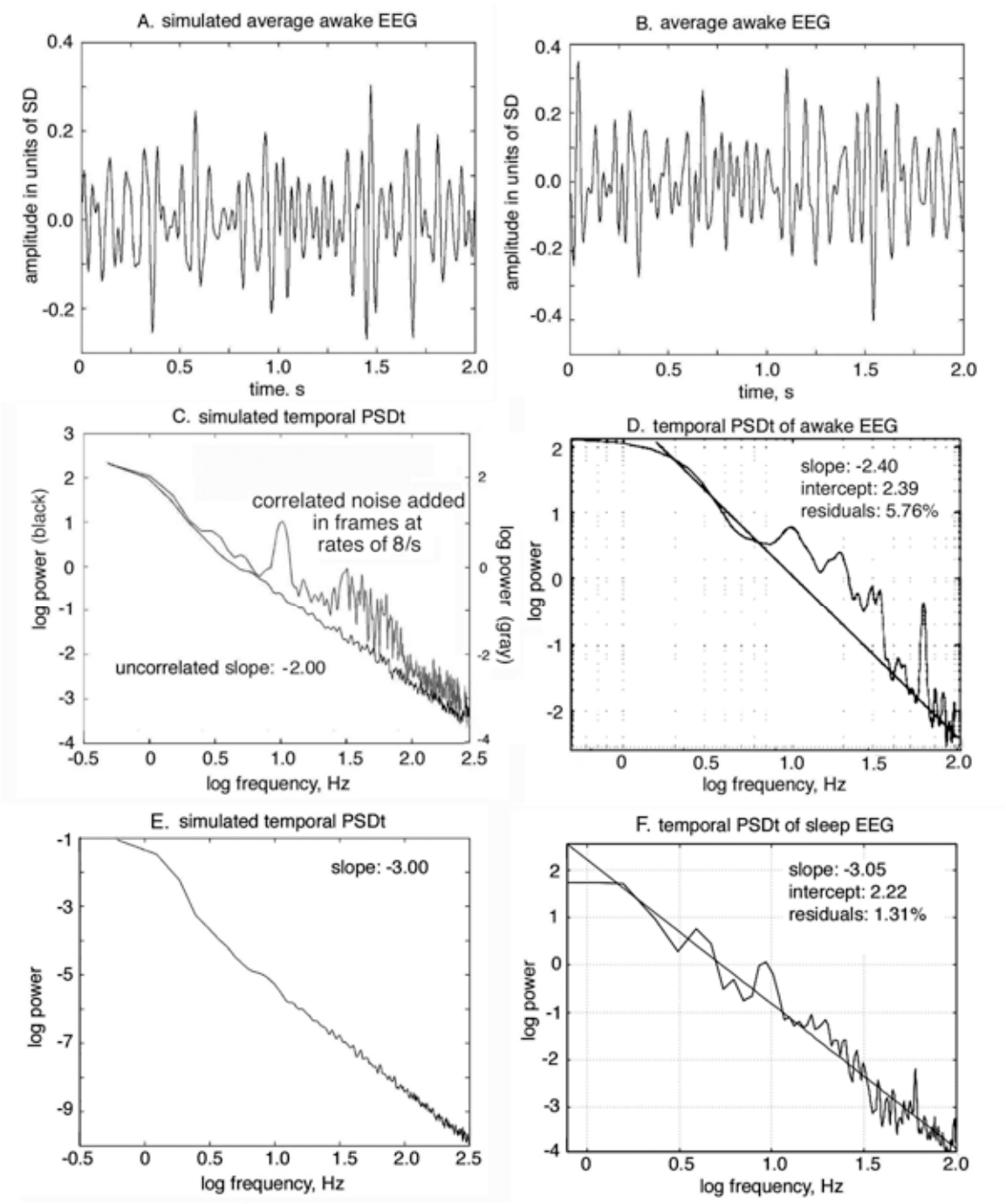

Fig. 1. A. Simulated beta EEG. **B.** Beta EEG from an awake human subject. **C.** Black curve: PSD_T of the uncorrelated noise, $\alpha = 1$ in equation (1); gray curve: PSD_T of intermittent segments with 90% spatially correlated noise (see Section 3.2 and Fig. 5, D). The beta and gamma peaks reflect carrier waves; the theta peak reflects repetitive state transitions, thus the unity of EEG structure across 1/f spectral energy. **D.** Average PSD_T from awake subject. **E.** Simulated EEG, $\alpha = 1.5$. **F.** EEG from human subject asleep [Freeman et al., 2005]. Use of log-log coordinates to display EEG spectra is essential for understanding EEG dynamics.

First, the pyramidal cells in hypercolumns were assumed to be aligned perpendicular to the array at the cortical surface. During EEG recording the sulci were avoided by making the 8x8 square array small enough (1x1 cm) to fit onto a single gyrus [Freeman et al., 2000; Freeman et al. 2005]. The cell bodies were assumed to form a layer parallel to the flat surface of the array, x, y, at a fixed cortical depth, $-\delta_1$, in the z dimension. Their synaptic currents were assumed to enter (or leave) the cells on one side (sink or source) and to leave (or enter) the cells (source or sink) on the other side of the layer of cell bodies. The source at any instant was represented by a fixed positive charge at a distance, $-\delta_2$, from the cell body layer toward the epicenter above the hypercolumns, and the sink was represented by a fixed negative charge at a distance, $+\delta_2$, from the cell body layer away from the surface. The electrode sites were assumed to lie in a square matrix at equal intervals, δ_3, in the x, y surface dimensions.

Second, on the assumption of fixed isotropic specific impedance of cortical tissue, Coulomb's Law served to calculate the relation of the potential at the surface to the distance of each recording point from each pair of point charges representing source-sink densities at each instant of magnitude q and of opposite sign separated by 2δ (not a point dipole) [Freeman, 1975/2004]. This relation was the point spread function (PSF):

$$v(x_j,y_j) = \sum_{o=1}^{o=64} \{q_o /[(x_j-x_o)^2 + (y_j-y_o)^2 + (\delta_1-\delta_2)^2]^{0.5} - q_o /[(x_j-x_o)^2 + (y_j-y_o)^2 + (\delta_1+\delta_2)^2]^{0.5}\}, \quad (2)$$

where v represented simulated EEG amplitude at x_j,y_j on the recording surface, x_o,y_o signified a specific location in a 15x15 matrix that embedded the 8x8 generating surface, and q_o was determined by the filtered random number at each location. The locations of surface points were spaced in accord with δ_3. The potentials were normalized by dividing them by the maximal value, which obviated the need for mirror charges to represent the effect of the non-conducting array surface. This point spread function (PSF) was comparable to the spatial impulse response [Freeman, 1975/2004] for a single active neighborhood (Fig. 2, A and C).

The values for $\delta_1 = 0.8$ mm and $\delta_2 = \pm 0.17$ mm were established for prepyriform cortex and olfactory bulb in cat and rabbit [Freeman, 1975/2004] by measuring surface distributions of potential on focal electrical stimulation and depth profiles, followed by simulations and curve fitting using Coulomb's Law. The PSD_X of the experimental and fitted PSF were compared with the PSD_X of neocortical EEG [Barrie, Freeman and Lenhart, 1996] and human intracranial EEG [Freeman et al., 2000]. The similarity of forms of PSD_X gave values of $\delta_1 = 1.0$ mm and $\delta_2 = \pm 0.2$ mm for the human neocortical PSF. The PSD_X were insensitive to variations in estimates of δ_1 and δ_2 on the order of ±20%. The values of $\delta_3 = 0.79$ mm (rabbit) and $\delta_3 = 1.25$ mm (human) were given by the interelectrode distances of the 8x8 arrays.

The random numbers from the 64 time series at each time step formed an 8x8 matrix, which was used to specify the intensity at each pair of point charges. The contribution of each pair of point charges to the surface potential was calculated by convolving it with the PSF over the 15x15 matrix using vector algebra. This operation simulated the smoothing effect of the volume conduction of dendritic currents upon extracellular recording at the pial surface.

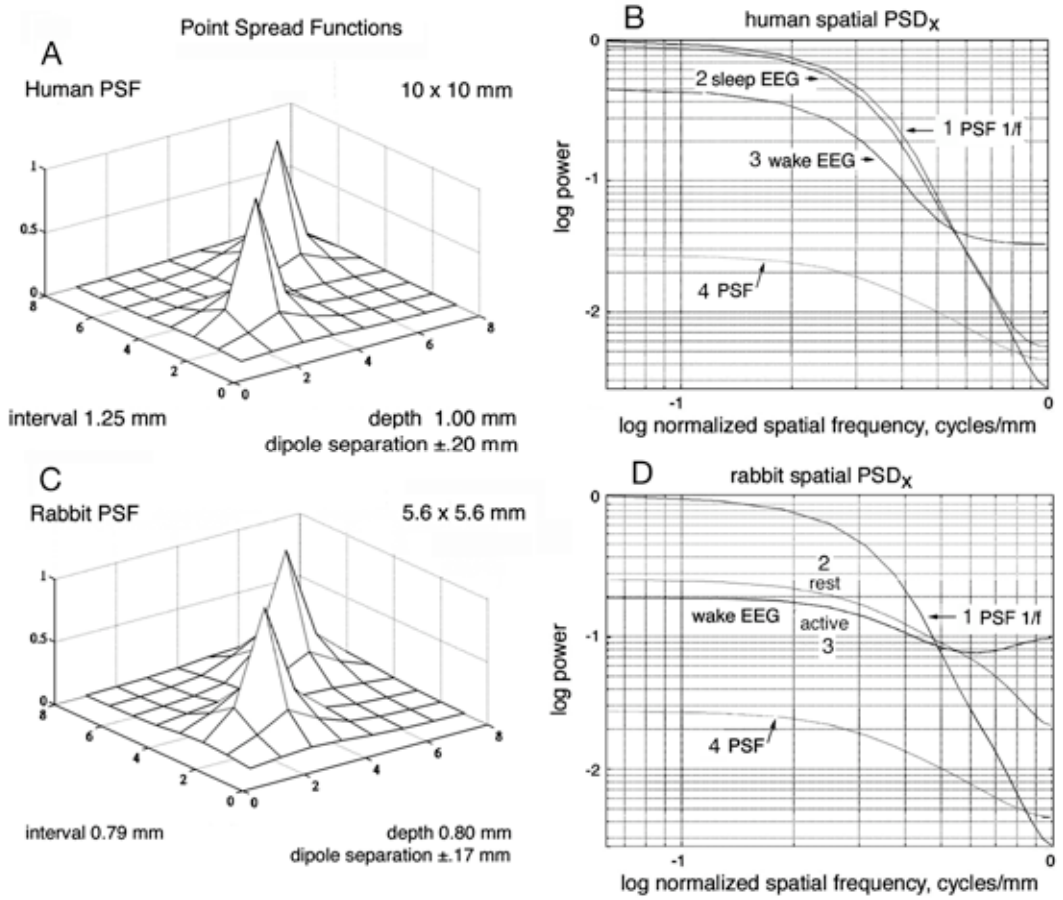

Fig. 2. A. The point spread functions (PSF) are shown for two locations with unit amplitude for the array dimensions in human (10 x 10 mm) and rabbit (5.6 x 5.6 mm).

B. Comparison of the normalized PSD_X of the PSF before 1/f spatial filtering (curve 4) and after 1/f filtering (curve 1) with the PSD_X of representative EEGs in human (asleep 2, awake 3) and rabbit (awake at rest, 2, active in conditioning, 3). The flattening was attributed to normalization of the PSD_X though the actual change in condition was substantial loss of power in high spatial frequencies in transition from awake to asleep [Freeman et al, 2005].

Third, simulation of PSD_X of EEGs in the sleep state required weighting in the real and imaginary spatial amplitude spectral domains by 1/f, just after 1/f weighting in the temporal spectral domain and before convolving the 8x8 matrix of 64 amplitudes at each time step with the 15x15 matrix for the PSF using vector algebra. At each time step the set of 8x8 amplitudes was embedded in 16 zeroes and transformed into the spatial frequency domain with the 2-D FFT [Freeman, 2004a,b]; the real and imaginary parts were filtered to give the 1/f amplitude spectrum using equation (1) with $\alpha = 1$; these two parts were transformed back to spatial set by the inverse FFT. The simulated spatial PSD_X from 50 time steps were normalized, averaged for display (Fig. 2, B and D) to compare the PSD_X in different behavioral states with each other and with the PSD_X of the PSF before the 1/f filter (curve 4) and after (curve 1).

2.3. Construction and classification of spatial AM patterns

The sequences of operations to generate and classify AM patterns are summarized in Table 1. Two sets of 64 time series were generated of sufficient duration to give 2 to 5 s of multichannel simulated EEG after truncation by FIR temporal filtering to extract the beta or gamma range:

uncorrelated noise in 64 independent time series and correlated noise in 64 replicates of the same time series independent of any of the time series in the first set. These two sets were combined by adding correlated noise to diminished uncorrelated noise in repeated frames, each lasting long enough to sustain ≥3 cycles at the peak frequency in the pass band. The time series duration was set to hold up to 40 frames with transition times between frames of 15%-25% of frame durations.

Table 1. Sequences of operations for construction of simulated AM patterns

Random numbers, Gaussian i.i.d, from one seed:
    64 independent time series, 1K-3K steps: "uncorrelated noise"
    64 replicates of 1 time series, 1K-3K steps, "correlated noise"
Temporal FIR band pass filter 0.1-100 Hz (analog filter on EEG)
Temporal 1/f filter – all states
Spatial 1/f filter – sleep state, not awake active state
Convolution with PSF to simulate volume conduction
Add 75% uncorrelated and 25% correlated for background state
Add 10% uncorrelated and 90% correlated for AM pattern state
Narrow band pass temporal filter: beta (15-20 Hz); gamma (40-45 Hz)
Amplitude modulation: 2 beta AM patterns; 2 gamma AM patterns
Construct 40 frames with ramps on and off forh 10 of each AM types

Sequence of operations for classification of simulated AM patterns

Temporal broad band FIR filter for beta (12-30 Hz) or gamma (25-55 Hz)
Hilbert transform to calculate vectorial order parameter: $\mathbf{A^2}(t)$
Calculate mean power at each step: $\underline{A^2}(t)$
Calculate rate of change of order parameter, $D_e(t) = \mathbf{A^2}(t) - \mathbf{A^2}(t-1)$
Calculate pragmatic information index: $H_e(t) = \underline{A^2}(t) / D_e(t)$
Calculate $\mathbf{A^2}(t)$ at time of maximal $H_e(t)$ in each frame as its feature vector
Display 40 locations of feature vectors in 64-space projected into 2-space
Classify 40 frames of the 4 types using Euclidean distance in 2-space

Each frame was ramped on and off in order to simulate the approximate 25-35 ms delay observed in the convergence of amplitude patterns to stable states [Freeman, 2003]; neocortical state transitions were not everywhere simultaneous but were distributed in time and space owing to conduction delays of the cortical axons mediating the transition [Freeman and Barrie, 2000; Freeman and Rogers, 2002]. Ramping was also required in order to avoid large spurious spikes in the analytic amplitude that were precipitated by large step changes in the signals to which the Hilbert transform was applied [Freeman, 2004a]. The parameters for generating the simulated EEG frames are summarized in Table 2.

The carrier waveform in each frame was modulated in amplitude on different channels over the full duration of the frame to create four AM patterns, prior to temporal AM. The amplitudes across the 64 channels (1 to 64) for the first 10 beta frames steadily increased from 0.37 to 1.0; the second 10 beta frames steadily decreased from 1.0 to 0.37. The spatial AM pattern in the first 10 gamma frames increased from 0.34 to 0.69 at midpoint and then decreased from 1.0 to 0.69. The AM pattern of the second 10 gamma frames decreased to channel 32 and then increased to channel 64 over the same range.

Table 2. Parameters for simulating background EEG and active EEG frames

Random numbers: Gaussian distribution with zero mean and unit SD
digitizing rate: 500/s (rabbit); 200/s (human)
1/f spectral weight for amplitude:
PSD_X, $\alpha = 1.0$;
PSD_T wake, $\alpha = 1.0$; PSD_T sleep, $\alpha = 1.5$.
Point spread function (PSF) to simulate volume conduction by vector convolution :
dipole depth: $\delta_1 = 0.80$ mm (rtabbit), 1.0 mm (human)
dipole separation: $\delta_2 = 0.17$ mm (rabbit), 0.20 (human)
interelectrode distance: $\delta_3 = 0.79$ mm (rabbit), 1.25 mm (human)
Mixtures:
background: 75% uncorrelated noise + 25% spatially correlated noise
active: 90% correlated noise + 10% uncorrelated
additive weights to create active frame: uncorrelated x 0.5 + correlated x 1.0
Properties of active frames:
duration of active states: 50 steps (100 ms, rabbit); 34 steps (166 ms, human)
interval: 62 steps (124 ms, 8 Hz, rabbit); 50 steps (250 ms, 4 Hz, human)
Ramp onset: begin at start of frame, decrease uncorrelated noise x 0.05/step in 9 steps while increasing correlated noise x 0.1/step (18 ms, rabbit, 45 ms human)
Ramp offset: begin ramp 9 steps before frame ending with same size increments
frames in each time series = 40; # types = 4 AM patterns; # cycles ≥3

Each simulation yielded 10 frames for each of 4 AM pattern types. The 64 amplitudes in each frame gave a 64x1 feature vector [König, 2000] that specified a point in 64-space. Amplitudes were calculated in four ways. The simplest was the root mean square (rms) of the filtered real part at each location and across each stabilized frame [Freeman and Burke, 2003]. Virtually the same results obtained from the gain coefficient of the FFT of the filtered EEG in the frame at the peak frequency. More effective was the mean analytic power, $\underline{A^2_{i,T}}(t)$ [Freeman, 2004b] of each channel, i, over the duration, T. Yet more effective was the analytic power of every channel at the moment of peak power in the frame. Preprocessing by Sammon's [1969] nonlinear mapping was the same as previously applied to EEGs [Barrie, Freeman and Lenhart, 1996; Barrie, Holcman and Freeman, 1999; Freeman, 2004a, b, 2005]. The 64 amplitudes formed a feature vector in 64-space for each of 40 frames. The mapping projected the 40 points from 64-space into a 2-D visualization plane for display, while preserving to a good approximation the distances between the points. To find the 2-D plane an initial plane was defined by the two coordinate axes with largest variances of the data. The $N(N - 1)/2$ Euclidean distances were calculated between the points in 40-space and between the points projected into the plane. An error function was defined by the normalized differences between the two sets of distances. The error was minimized by a steepest gradient descent procedure [Appendix 1 in Sammon, 1969; König, 2000; Freeman, 2005].

For classification a center of gravity was calculated for the 10 points of simulated AM patterns for each of the 4 types. Classification of each frame was determined by the shortest Euclidean distance to a center of gravity in 2-space. A summary % correct was calculated from the number

of correctly classified points divided by the total and multiplied by 100. Among pairs of clusters the binomial probability was used to compute the likelihood that the number of correct frames out of the total number of frames could have occurred by chance. For pair-wise classification a line was drawn visually that best separated the clusters displayed in 2-D on the premise of linear separability. For 4-way classification the goodness of classification was compared with the prior results from AM pattern classification of EEGs with respect to conditioned stimuli [Freeman, 2005].

The choice of the temporal band pass filters for beta and gamma was based on prior results for optimized classification of AM patterns with respect to conditioned stimuli [Table 3 and Fig. 5 in Freeman, 2005]. The filtering was guided by two considerations. First, the generator pass bands were narrow (e.g. 12-20 Hz for beta, 40-45 Hz for gamma), because experimental measurements of carrier frequencies [Freeman, 2003] showed that while the center frequency varied from one epoch to the next over broad ranges of 12-80 Hz, the variation of the frequency about its center within an epoch seldom exceeded 5-7% of the center frequency. Second, the pass band of the frequency range for observation and measurement of simulated AM patterns was broad (e.g., 12-30 Hz for beta, 25-55 for gamma), because of the wide variation in center frequencies. Setting the generated pass bands narrower than the measuring pass bands reduced the variation in measured parameters during correlated frames that could be ascribed to random interference between uncorrelated noise and correlated noise, when they had identical pass bands.

2.4. Calculation of amplitude, analytic amplitude, and cortical power

The analytic signal, a(t), is defined as a complex function:

$$a(t) = v(t) - i\,\mathcal{H}[v(t)] = v(t) - i\,u(t), \quad (3)$$

where i = square root of –1; the real part, v(t), is the EEG or simulated EEG after band pass filtering; and $\mathcal{H}$ is the Hilbert operator giving the imaginary part, u(t). The analytic amplitude, A(t), is given by the square root of the sum of squares of the real and imaginary parts:

$$A(t) = [v^2(t) + u^2(t)]^{0.5}, \quad (4a)$$

The analytic phase is given by the arctangent of their ratio:

$$\Phi(t) = \text{arctangent}\,[u(t)/v(t)]. \quad (4b)$$

As proposed in the Introduction, v(t) represented the current density of the excitatory neocortical pyramidal neurons, and u(t) in quadrature represented the current density of the inhibitory interneurons, which was the output of the feedback limb of the cortical negative feedback loop. On average the oscillations of the inhibitory neurons lagged the oscillations of the excitatory neurons by $\pi/2$ rad [90°, Freeman, 1975/2004], thereby justifying use of the Hilbert operator. Analytic power was given by the square of analytic amplitude, $A^2(t)$, because it was proportional to the square of the extracellular dendritic current flowing across the relatively fixed extracellular tissue resistance, I^2R, including synaptic current from both forward (excitatory) and feedback (inhibitory) neural populations (Freeman, 2004a,b). This was an approximation, because most of the neural energy was dissipated in flows across the high transmembrane impedances matched between synapses and trigger zones, which were not fixed, yet the same synaptic currents that controlled cortical pulse outputs produced the IR voltage differences seen in the EEG as they flowed across the relatively invariant low impedance tissue return path.

Distributions of analytic phase, $\Phi(t)$, provided estimates of temporal synchrony for selected frequency components. A complementary method that relied solely on analytic amplitude gave

an estimate of synchrony, $R_e(t)$, for aperiodic oscillations in a moving window [Freeman, 2004a]. The peak frequency of the filtered data was calculated from the FFT of the spatial ensemble average of the 64 $A_j(t)$. A sliding window of duration twice the wavelength of the peak frequency of the FFT specified the window order in digitizing steps, T; it was stepped along the $A_j(t)$ at the digitizing interval. The standard deviation of $A^2_{j,T}(t)$ in the window was computed for each channel to get the mean of the 64 $SD_{i,T}(t)$ across channels, $\underline{SD}_T$. The spatial ensemble average, $\underline{A}_T(t)$, of the 64 time series of $A_j(t)$ in the window was computed to get its SD_T. Their ratio, $R_e(t)$, was plotted with the midpoint of the window at time t.

$$\underline{SD}_T(t) = 1/64\ \Sigma\ SD_{j,T}(t),\ \ j = 1, \ldots, 64, \qquad (5a)$$

$$R_e(t) = SD_T \text{ of mean } \underline{A^2}_T(t) \text{ / mean } \underline{SD}_T \text{ of } A^2_j(t). \qquad (5b)$$

The range was 1 for perfect synchrony to $1/T^{0.5}$ for complete independence. In order to compare the time relations of $R_e(t)$ to the other measure of synchrony, SD_X, the ratio was inverted, $1/R_e(t)$. Low values showed time periods of high synchrony; high values reflected desynchronization.

Measurement of AM patterns required finding a value for the signal on each channel in each frame and constructing a 64x1 feature vector. That feature vector was adopted as a vectorial order parameter, because it expressed quantitatively the self-organized patterning that emerged from the background with the transition by which each new AM pattern formed. The order parameter, $\mathbf{A^2}(t)$, specified a point in 64-space for each frame. The reliability of the peak value of $\mathbf{A^2}(t)$ to specify the AM pattern over the duration of the frame was estimated by the rate of change in the order parameter, $D_e(t)$, which was approximated by calculating the scalar Euclidean distance in 64-space between successive points with each digitizing step [Freeman, 2004b, 2005],

$$D_e(t) = |\mathbf{A^2}(t)| - |\mathbf{A^2}(t\text{-}1)|. \qquad (6)$$

The stability of an AM pattern within its frame gave low values of $D_e(t)$, whereas the transition from each AM pattern to the next gave high values between frames.

The mean power, $\underline{A^2}(t)$, tended to high values within frames and to low values between frames. For classification purposes the 64 values were normalized to zero mean and unit SD, because the mean might increase or decrease from the background level with each new frame and had no classificatory value [Freeman and Grajski, 1987]. The feature vector was calculated from the peak analytic power in each frame at the time point with minimum rate of change in the order parameter and maximum power. That time point was located by use of an index, $H_e(t)$, called the 'pragmatic information index' after [Atmanspacher and Scheingraber, 1990], which was defined as the ratio of the mean rate of energy dissipation, $\underline{A^2}(t)$, to the rate of change, $D_e(t)$, in the order parameter, $\mathbf{A^2}(t)$:

$$H_e(t) = \underline{A^2}(t) / D_e(t). \qquad (7)$$

The distribution of $\log_{10}[H_e(t)]$ was close to Gaussian; hence classification using $H_e(t)$ for frame localization and $\mathbf{A^2}(t)$ feature vectors required empirical determination of a threshold value for $H_e(t)$. That was done by constructing tuning curves to find the optimal value for best classification [Freeman, 2005]. Maximal correct classification of frames obtained for feature vectors at time steps coinciding with peak values of $H_e(t)$.

3. Results

3.1. Simulation of the background EEG with filtered random numbers

The simulated time series, v(t), (Fig. 1, A) conformed by visual inspection to the EEG whether unfiltered or filtered in the gamma or beta ranges (as shown in B). The PSD_T with $\alpha = 1$ in the background state conformed to $1/f^2$ (C), which was not seen in the awake EEG (D), had multiple peaks deviating from a fitted line, $1/f^2$. Simulation of those peaks required inclusion of correlated noise that conforming to the active state (gray curve in (C); see Section 3.2, Fig. 6).

The PSD_X of the random numbers was spiky but essentially flat as expected for white noise. The point spread function (PSF) was calculated to simulate the smoothing at the recording surface by volume conduction of the random activity simulated at the depth specified in equation (2) (Fig. 2, A and B). The PSD_X of the PSF (curve 4 in Fig. 2, B and D) failed to simulate the PSD_X because their narrow range of log power was insufficient. When the random noise amplitude was weighted by equation (1) with $\alpha = 1$ in the spatial frequency domain, its PSD_X (curve 1 in B and D) then coincided with the PSD_X of the human EEG in sleep (curve 2 in B). The PSD_X of the EEG in the awake human (curve 3 in B) and rabbit (curve 3 in D) showed narrower ranges in log power though not as narrow as those from PSF. The histograms of the simulated amplitude values and of the EEG amplitude values were all close to Gaussian. The histograms in semi-log coordinates of the square of the analytic amplitude, $A^2(t)$, of EEG (D) were also Gaussian, but those of the simulated $A^2(t)$ were skewed with a tail of low values.

The distributions of eigenvalues of EEG under PCA (for an example in Section 3.2, see Fig. 5, B) were similar in awake and sleep states (Table 3) with a high percentage of the variance in the 1st component (grand mean and SD 76.3% ± 6.67). The distribution of eigenvalues of the uncorrelated noise after convolution and 1/f weighting was much broader than that of the EEG data (grand mean of % variance in the 1st component 24.0% ± 4.2%). By this criterion the simulated background EEG had to be a mix of uncorrelated and correlated noise; a good approximation was obtained with a mixture of 75% uncorrelated noise and 25% correlated noise.

The Hilbert transform of the mixture for background gave the analytic amplitude by equation (4a), shown by the mean across 64 values at each time step (black curves in Fig. 3, A and B) and the analytic phase by equation (4b). Successive differences in analytic phase across the 64 phase values at each time step were used to calculate their spatial $SD_X(t)$ of differences as a time series. For uncorrelated noise the $SD_X(t)$ was uniformly high, whereas for background mixtures containing correlated noise the $SD_X(t)$ showed intermittent spikes (gray curves in Fig. 3, A and B). These spikes were defined as coordinated analytic phase differences, CAPD (Freeman, Burke and Holmes, 2003). The high values of CAPD designated times of phase slip; the low values designated intervening frames. In both the simulated EEG (illustrated for beta in Fig. 3, A) and observed beta EEG (B) the analytic amplitude tended to low values during phase slip and to high values within frames. These relations held whether the simulated phase was calculated by the Fourier or Hilbert methods. These epochs were designated “frames” for their similarity to frames in the EEG [Freeman, 2005]. The mean analytic amplitude squared, $\underline{A}^2(t)$, of the simulated signals was four-fold smaller than that of the EEG as a consequence of normalization.

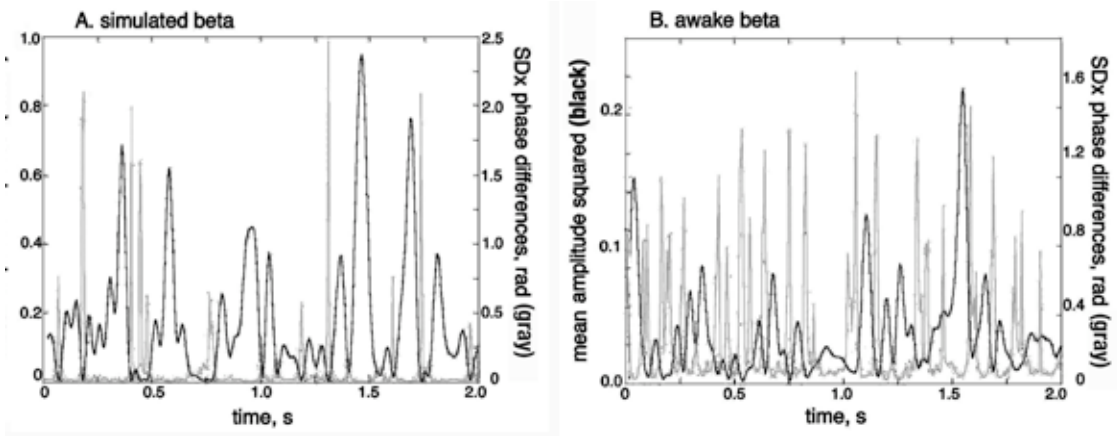

Fig. 3. The inverse relation is demonstrated between mean analytic amplitude, $\underline{A}(t)$, and the spatial standard deviation, $SD_X(t)$, of the analytic phase at each digitizing step for both the simulated data and the EEG. This inverse correlation occurred only to the extent that the noise was correlated across the 64 channels, because jumps in phase (phase slip) had differing size and sign in uncorrelated time series giving high $SD_X(t)$, while correlated time series all changed together and gave low $SD_X(t)$.

A significant difference between simulated background and EEG in the active state was revealed by calculation of the rate of change in the order parameter, $D_e(t)$, by equation (6), which served as a measure of spatial amplitude pattern stability. The real and simulated values of mean and SD for $D_e(t)$ (calculated after taking the logarithm, Fig. 4, C, D) did not differ significantly. However, the simulated background time series (Fig. 4, A) showed a sustained level of minima well above unity, from which spikes occurred usually in conjunction with minima in $A^2(t)$, whereas the EEG showed epochs of values well below unity (B). Those epochs gave a skewed distribution to log $[D_e(t)]$ from EEG with a tail of low values (D). The histogram of simulated log $[D_e(t)]$ had a skewed distribution with a tail of high values (C).

This phenomenon extended into the performance of the index for pragmatic information by equation (7). The peaks in $H_e(t)$ occurred during minima of phase variance by all measures (Fig. 4, E, F compared with A, B). The mean values from the EEG exceeded those from the simulated time series by an order of magnitude (G, H) with skewing of the distribution of the simulated data (due to the skew in $D_e(t)$) but not that of the EEG. Clearly the simple steady-state 1/f noise failed to fully simulate the full range of statistical properties of the normal EEG in the awake state because of skewness in $\log[D_e(t)]$. Adequate simulation required inclusion of episodes of correlated noise to represent active states in the EEG.

3.2. Simulation of state transitions by interspersing correlated and uncorrelated frames

A second set of 64 simulated EEGs was constructed by 64 replications of a single noise time series. Independent noise was added to each of the 64 identical time series in the form of uncorrelated random numbers with SD = 0.1 (the variance was 10% of the total variance). The PSD_T and PSD_X were unchanged. PCA gave 98.9 ± 0.2% of the variance in the 1st component (Table 3), far exceeding values seen in EEGs. Therefore, EEGs in active states were simulated by mixing uncorrelated noise with correlated noise in varying ratios (Table 2).

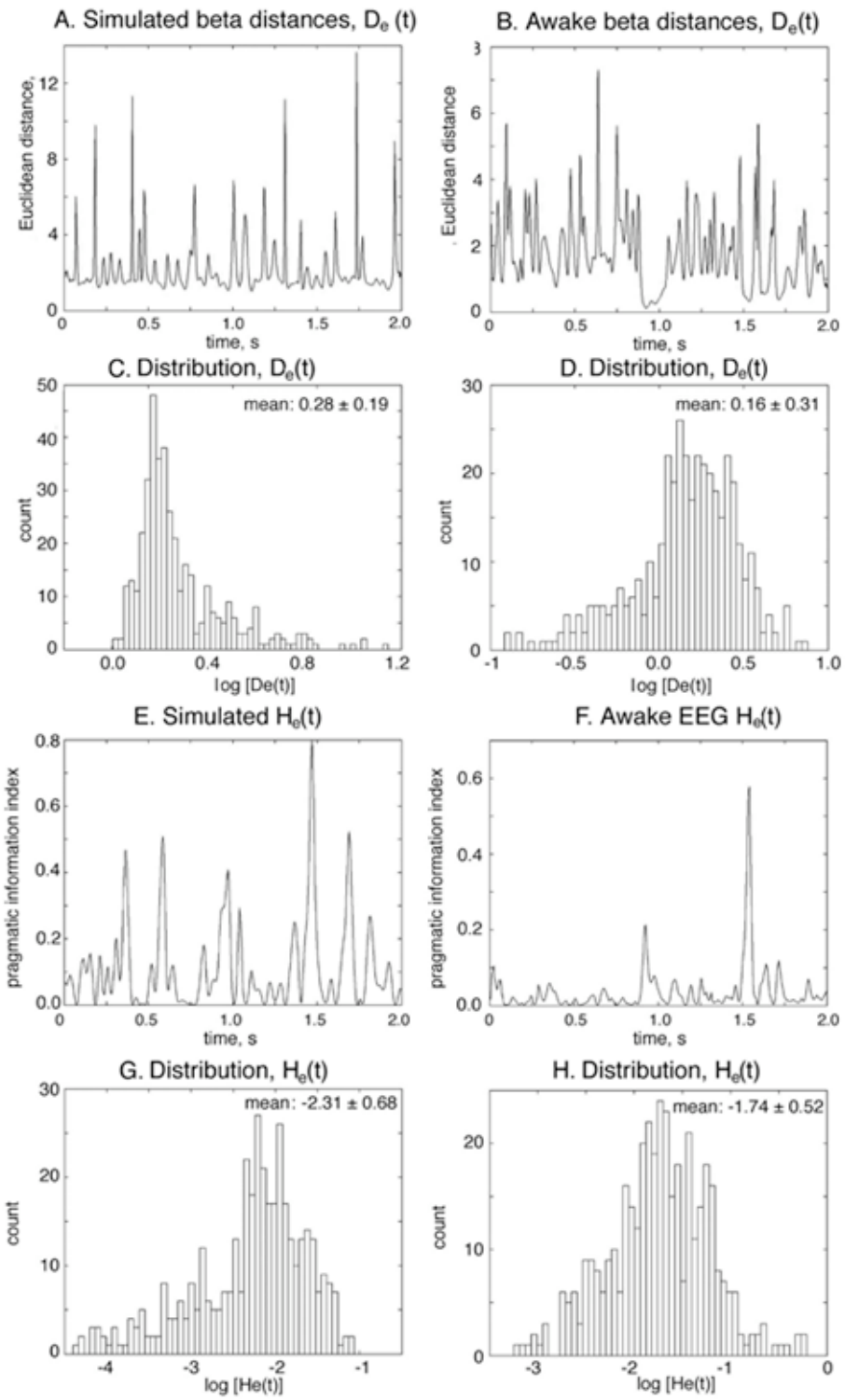

Fig. 4. A. Comparison of Euclidean distance measure of stability, $D_e(t)$, from simulated and human EEGs.

B. Comparison of measure of pragmatic information, $H_e(t)$, from simulated and human EEGs.

Further development of the simulation required introduction of repetitive state transitions to simulate an active state to contrast with the background state. The results to this point were used to design simulations of neocortical EEG at alternating levels of low and high levels of synchrony (Fig. 5, A), which were needed to simulate cortical state transitions as revealed by the EEG. The background EEG was again simulated by the sum of 75% uncorrelated noise plus 25% correlated numbers to approximate the distribution of % variance from PCA of the EEG. The resulting values of the 1st component (Fig. 5, B) were intermediate between values from uncorrelated noise and correlated noise (Table 3) but less than values from the EEG.

The presumed "active" state of neocortical EEG was simulated by the introduction of frames of 90% correlated noise with 10% of the variance from uncorrelated noise (Table 2). Each frame was simulated by reducing the background amplitude by 50% and adding correlated noise. The correlated noise was first band pass filtered in either the beta range or the gamma range (15-20 Hz or 40-45 Hz). Ramping mitigated the edge effects of the abrupt state change. To simulate human EEG a sequence of 8 frames was inserted into a background epoch of 2 s, each frame lasting 170 ms (34 steps at 5 ms) and separated by 80 ms (16 steps) with a recurrence interval of 250 ms (50 steps, 4 Hz, Fig. 5, A). Comparable parameters were used to simulate rabbit EEG (15 frames, duration 100 ms, 50 steps at 2 ms digitizing step, recurrence interval 125 ms, 8 Hz (Fig. 1, C and Fig. 5, D). The Hilbert transform was applied to the 2 s to 4 s epochs, and the parameters for detecting phase slip were calculated as in Section 3.1.

The 1/f PSD_T of the uncorrelated noise (Fig. 1, B, gray) was modified by the appearance of spectral peaks in the theta, beta and low gamma ranges (B, black), similar to those illustrated for the human EEG in the awake state (Fig. 1, D). The PSD_X of the 75%-25% background (Fig. 5, C, gray curve) showed slight loss of high frequency power compared with that from the 100% uncorrelated noise (Fig. 2, B, gray), whereas the PSD_X of simulation of active EEG had substantial loss of power in mid-range spatial frequencies (C, black), as did the PSD_X of human and rabbit EEG (Fig. 2, B, D) in the awake state. The time base in Fig. 5, D was extended to 4 s to show the transition from slow wave background activity to higher frequencies with onset of the active state.

Results of calculating simulated EEG parameters using the Hilbert transform are shown in Fig. 6 for a case in which the correlated noise was generated in the beta range, 15-20 Hz. For the blue curves the pass band for display was also in the beta range (12-30 Hz), whereas for the red curves the pass band was in the gamma range (25-55 Hz). The aim of this test was to determine how well the parameters distinguished frames with power concentrated within either of these two ranges. This test was required in order to simulate the classification of beta vs. gamma spatial patterns of EEG in rabbit neocortex with respect to classes of conditioned stimuli [Table 3 and Fig. 5 in Freeman, 2005]. The duration of each frame (170 ms, 34 bins) was set to give at least 3 cycles of oscillation, which had been found to hold for frames in rabbit EEG that could be classified with respect to stimuli. The recurrence intervals were set to give a peak in the theta range, here 4 Hz (Fig. 5, B). Correlated noise onsets and offsets were ramped up and down in 9 steps of 0.1; uncorrelated noise was ramped down and up in steps of 0.05 at onset-offset, in order to simulate the near-one-cycle lags in the emergence of AM patterns that could be classified with behavior as seen in EEG frames [Freeman, 2003].

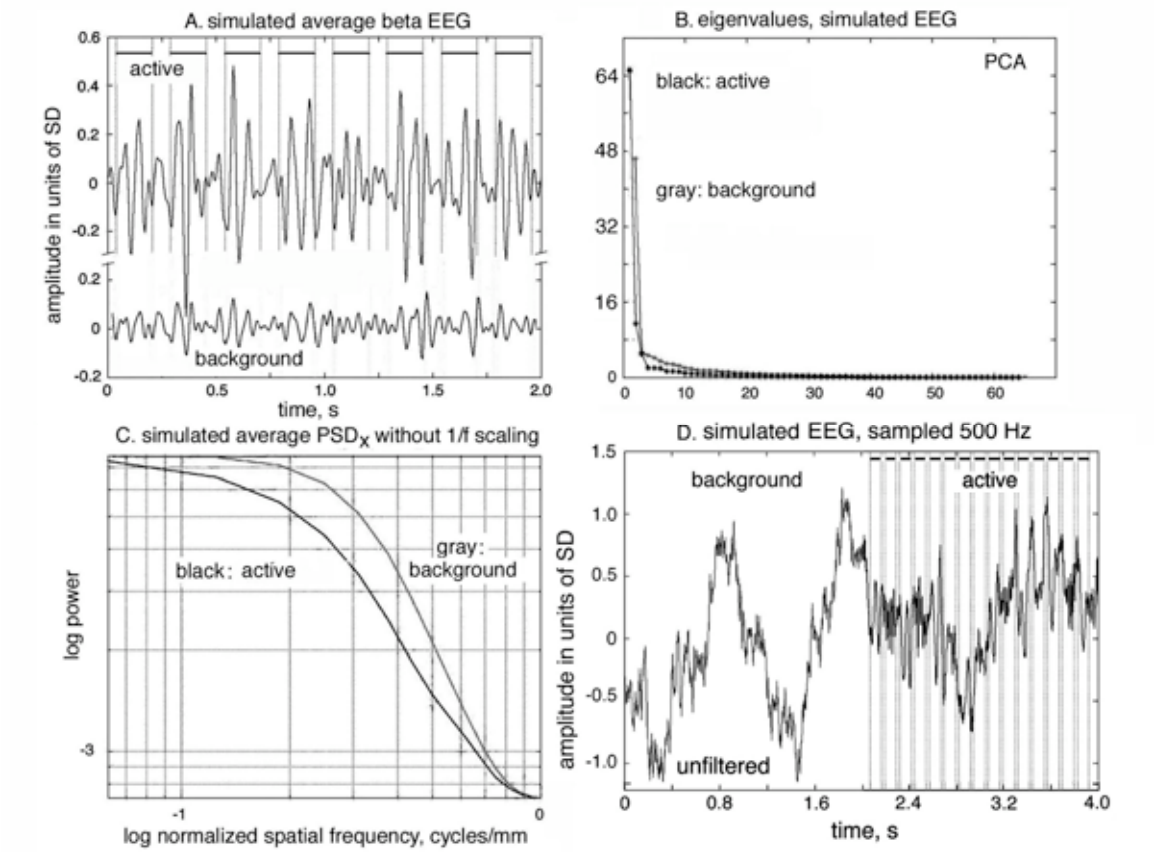

Fig. 5. A. Comparison of simulated background (gray) and active (black) EEGs in the beta range. The simulations of the PSD_X were done without 1/f weighting in the spatial domain. **B.** Simulation of rabbit EEG in 2-s epoch of background followed by 2-s epoch of an active state with alternating frames of beta (15-20 Hz) and gamma (40-45 Hz) activity, each lasting 100 ms and separated by 24 or 26 ms, with repetition at 8/s.

The bars at the top of each frame in Fig. 6 show the locations in time of 8 frames of enhanced correlation. The spatial standard deviation of analytic phase differences, $SD_X(t)$, tended to form low-valued plateaus of coordinated analytic phase differences (CAPD) during the frames for both band pass filters (A), with little difference between them. The same characteristics held for the Euclidean distances, $D_e(t)$ (B). The distribution of values of $D_e(t)$ was close to normal. The pragmatic information index, $H_e(t)$, gave high peaks when the pass band of the observation overlapped the pass band of the signal (C, blue), but not when the two pass bands did not overlap (C, red). The ratio of the mean variance of the 64 signals to the variance of the mean signal, $1/R_e(t)$, gave sustained low plateaus in the frames of high correlation, notably more so with the temporal pass band for observation (12-30 Hz) set to the frequency range of the generated signal (15-20 Hz, D, blue curve).

Table 3. Distributions of % variance of 1st component of PCA

Pass Band	Awake EEG	Asleep EEG	Uncorrelated noise	Correlated noise
Beta	81.0±4.3	74.5±7.4	24.1±1.5	98.9±0.2
Gamma	74.4±4.4	73.6±6.7	12.7±1.3	98.9±0.3
Unfiltered	77.0±8.1	77.6±8.4	45.1±9.4	98.4±1.4

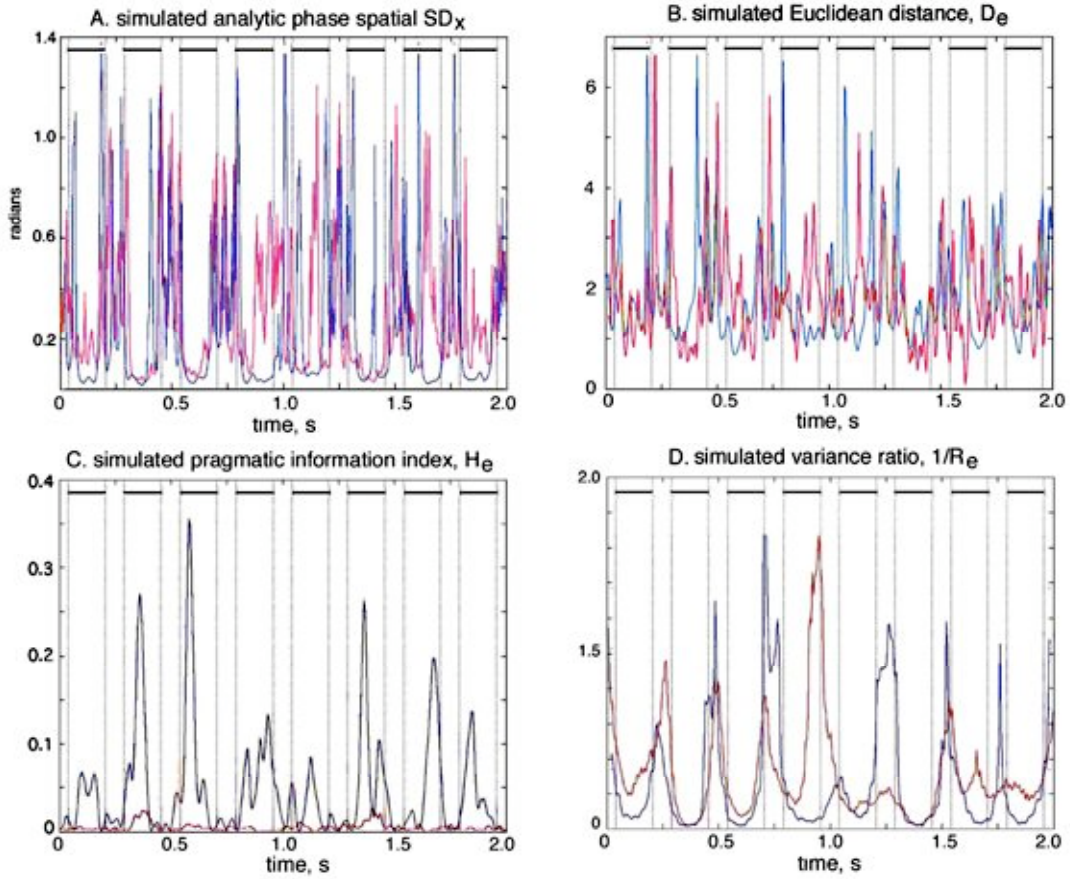

Fig. 6. Display of parameters calculated from simulated beta frames generated at 15-20 Hz and detected with a beta pass band (12-30 Hz, blue curves) vs. a gamma pass band (30-80 Hz, red curves). **A.** $SD_X(t)$ (A). **B.** $D_e(t)$. **C.** $H_e(t)$. **D.** $R_e(t)$.

The peaks in $H_e(t)$ during simulated frames of enhanced correlation varied markedly, and their durations were substantially less than the durations of the generated frames, which were well captured by the durations of the troughs in $1/R_e(t)$. These phenomena were commonly seen in rabbit neocortical EEG, particularly the foreshortening of the duration of peaks in $H_e(t)$ in comparison to the duration of frames by other measures [Freeman, 2003, 2004a,b, 2005]. The variations in $H_e(t)$ and in $\underline{A}(t)$ were accentuated when the pass band of observation was made identical with the pass band of generation. The correlated and uncorrelated time series, having been constrained by similar pass bands (beta or gamma), ran in and out of phase maximally when the generating and observing pass bands coincided. The details of the heights and shapes of the peaks differed on repetitions with differing seeds for the random numbers used to simulate noise, but the locations of the frames were easily replicated with differing seeds (Fig. 7).

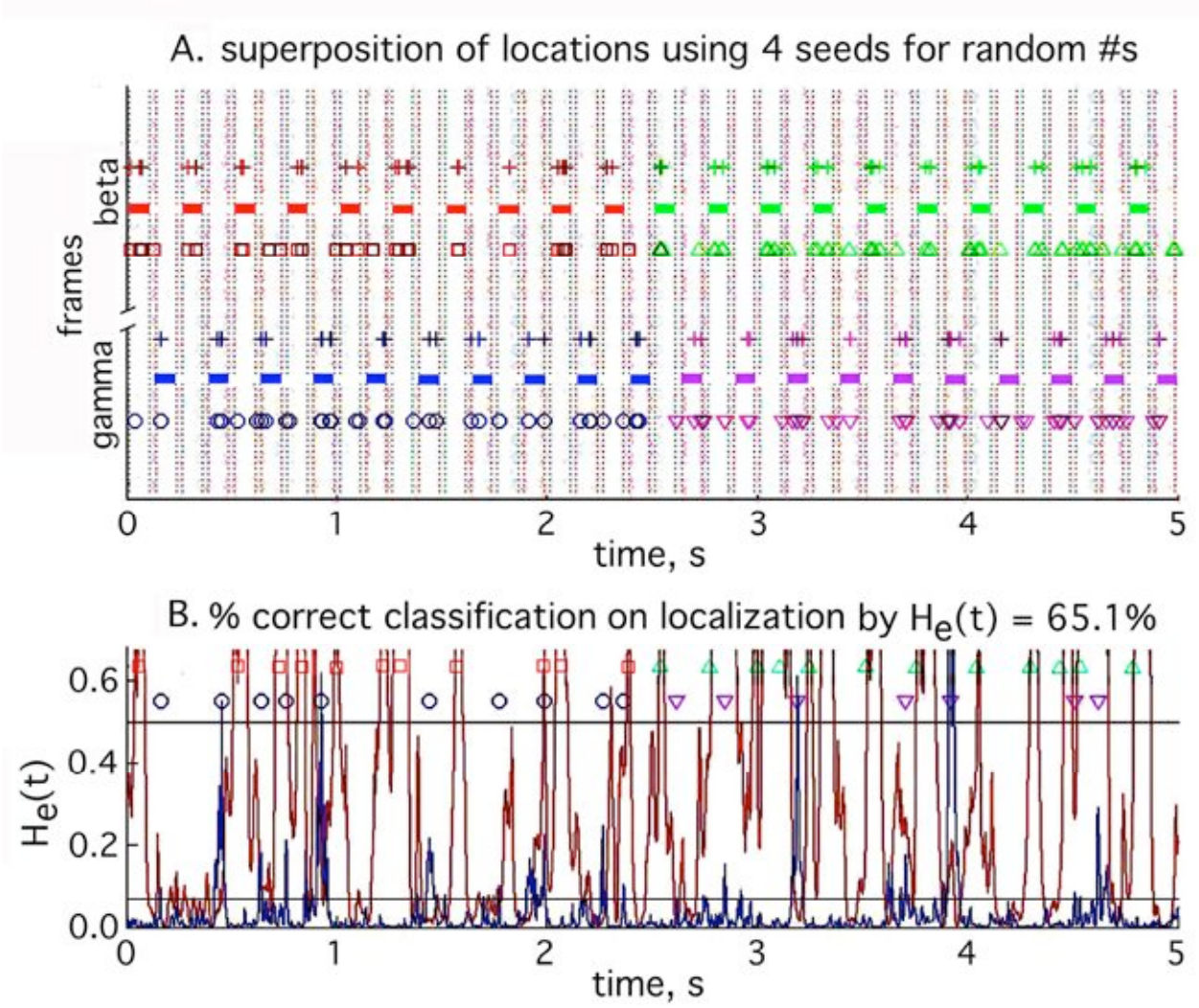

Fig. 7 A. The vertical dotted lines show the start and end of frames. The bars (red, green, blue, violet) locate 4 types of AM patterns; red-green = beta (15-20 Hz); blue-violet = gamma (40-45 Hz). Upper set: beta pass band (12-30 Hz); lower set: gamma pass band (25-55 Hz). The 4 symbols (□ Δ O ∇) show the locations of threshold crossings for four replications using different seeds for new sets of random numbers. The crosses (+) show time locations of the peaks of $H_e(t)$ at which feature vectors, $\mathbf{A}^2(t)$, were calculated.

B. One classification run is shown. $H_e(t)$ is from the beta pass band (red) or the gamma pass band (blue). The thresholds for $H_e(t)$ (black lines determined by trial-and-error) were used to locate empirical times of onset of AM patterns indicated by the 4 plotting symbols. Feature vectors, $\mathbf{A}^2(t)$, were determined at the times of the maximal value of $H_e(t)$ in the time interval to the end of the current frame. Classification was by Euclidean distance after nonlinear mapping (Fig. 8).

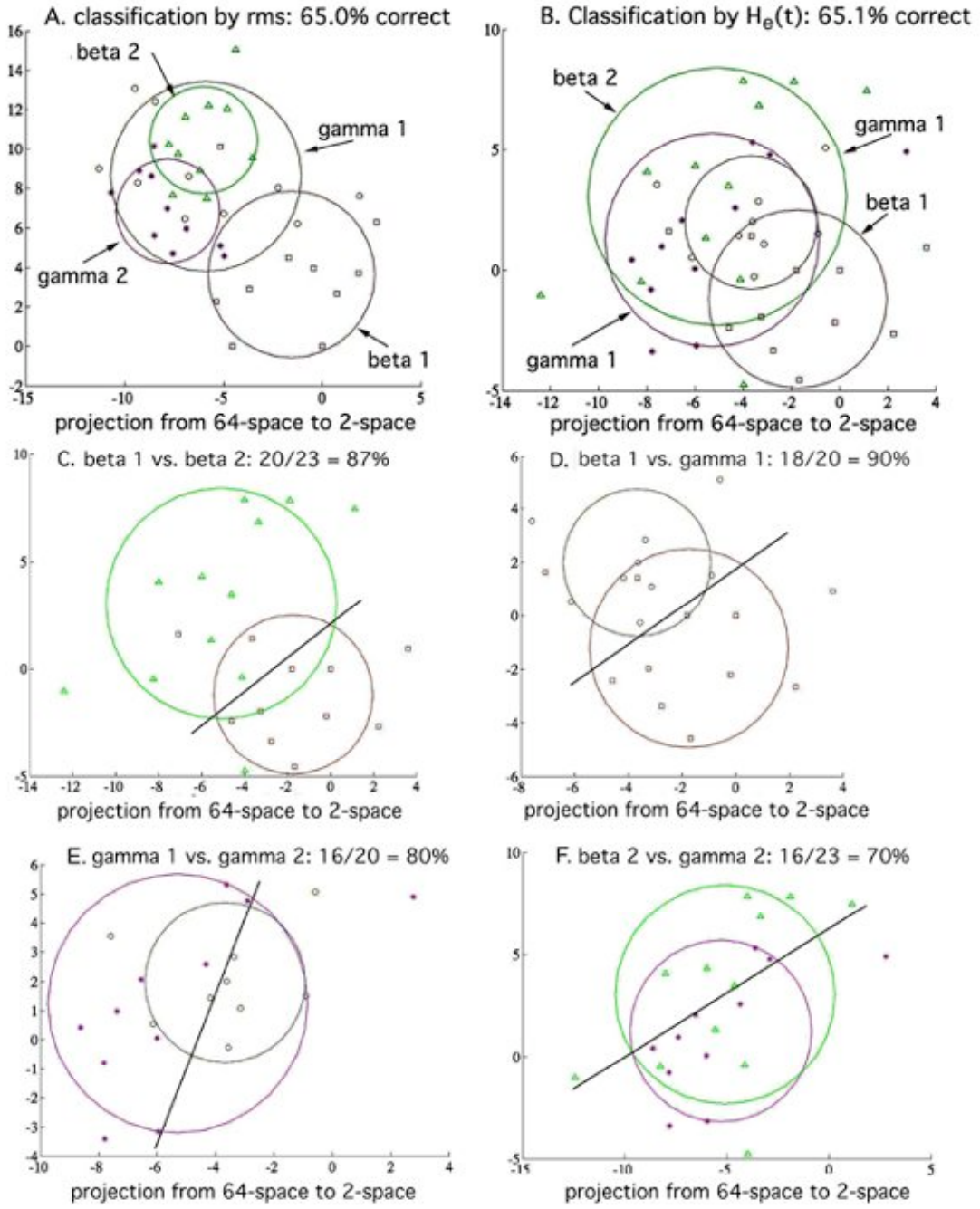

Fig. 8. Classification after nonlinear mapping [Sammon, 1969] was by finding the shortest distance for each point to the 4 centers of gravity. **A.** The 64x1 feature vector was the root mean square (rms) amplitude of the simulated EEG, v(t), for each channel over the 50 time steps in each frame.

B. The feature vector was the analytic amplitude squared, $A^2(t)$, at the maximal value of $H_e(t)$ in the 50-step window following a threshold crossing of 0.5 (beta) or 0.08 (gamma).

C-F. Pair-wise classification was based on the assumptions of linear separability and independence of each pair.

3.3. Simulation of spatial patterns of amplitude modulation (AM patterns)

The length of the generated epoch was 5 s plus 800 ms to allow FIR filtering (Fig. 7, B). The background EEG at rest had been simulated in prior runs of 4 s by omitting high correlation frames in the first 2 s. To simulate a full active state there were 40 frames in the 5 s with carrier frequencies generated alternately between 15-20 Hz and 40-45 Hz. The 100-ms frames were separated by 24-26 ms with no overlap. The values for $H_e(t)$ were calculated on two separate runs for using the beta and gamma pass bands of 12-30 Hz and 30-80 Hz. The values of $H_e(t)$ were superimposed in a graph (Fig. 7, B) with the two thresholds differing by a factor of 10, serving to demonstrate first that peaks did occur in the background epoch but sparsely, and that the high peaks in the active epoch tended to alternate in accord with the locations of the 20 frames generated in each of the two ranges for carrier waves. In order to achieve the levels of correct classification found for the EEG [Freeman, 2005], and in conformance with the replication of PSD_X (Fig. 2, D), it was necessary to omit the spatial 1/f filter of the random numbers.

This method created 40 AM patterns: 10 each of 4 AM patterns, which were preprocessed by nonlinear mapping [Sammon, 1969; Barrie, Holcman and Freeman, 1999; König, 2000] and classified by Euclidean distance in 2-D display space, as had been the AM patterns derived from EEG analysis [Freeman, 2005]. The 4-way classification was first done using the 64 rms values of amplitudes, v(t), averaged over the known 50 steps in each frame. The 64x1 feature vectors specified 40 points in 64-space, which were projected into 2-space for display (Fig. 8, A). Circles were used to show the SD in display space of the 4 groups about their centers of gravity. Classification was deemed correct when the distance of each point was shortest to its corresponding center. The % correct classification by rms was 65.0%.

The test was then conducted not using the known time markers but using $H_e(t)$ to locate the frames in the same manner as for the unknown locations of EEG AM patterns [Freeman, 2005]. A threshold value of was set by trial-and-error for data from the beta and gamma pass bands (usually differing in correspondence with 1/f), and a 100 ms window was initiated at each positive crossing of $H_e(t)$ above that threshold. The time location of the maximal value of $H_e(t)$ in that window served as the time marker at which to take the 64 values of $H_e(t)$ at the point as the feature vector for that frame. Numbers of flagged frames ranged from 32 to 46 for different seeds with an average near 40. Classification by distance to centers gave an average of 62±3% (Fig, 8, B) in patterns that replicated those obtained for AM patterns from EEG [Fig. 4 in Freeman, 2005]. The values of % correct approximated those in 4-way classification of AM patterns [Table 2 in Freeman, 2005]. Pair-wise classification was done by passing a line to optimally separate the displays of points on the assumption of linear separability (Fig. 8, C-F). The mean % correct was 81±5%, which replicated prior results with this measure of 71.7% to 74.2% [Table 1; see also Fig. 2, B and Fig. 4, C, D in Freeman, 2005]. The test was replicated with 4 different seeds to give four independent sets of random numbers. Correct classification by rms feature vectors averaged 63±3%, compared with 65.2% to 69.1% for EEGs [Table 2 in Freeman, 2005].

An alternative method for evaluation of classification was afforded by knowledge of the actual locations of the simulated AM frames, which had not been possible for AM patterns in the EEG. The location in time of the start of each frame was plotted as a colored symbol at the point where $H_e(t)$ crossed a threshold (Fig. 7, A), and a cross was plotted at the time when the maximal value

of $H_e(t)$ occurred, at which the feature vector was evaluated from $A^2(t)$, on a grid that indicated the time lines of the generated frames (Fig. 7, B). The number of observed frames that were located within the generated time slots, had the correct AM type and had the correct generated carrier frequency was divided by the total number of frames detected by threshold crossings. The test was repeated with 4 seeds for random numbers. The average % correct was 70±3%, which was consistently higher than the classification by Euclidean distance. The overlaid plots gave an indication of the degree of variability in location of frames with respect to the generated AM patterns (the solid bars in Fig. 7, A). This test revealed that on average there were 12 frames that were missed by $H_e(t)$, and 15 frames were reported when none ought to have been found. These numbers from the 40 generated appeared to correspond to the approximate 65% of correct classifications, because some of those incorrect were actually correct but assigned to times outside the boundaries of the generated amplitude patterns.

4. Discussion

This method of simulation is based on the premise that EEG activity is due to near-white noise generated by immense numbers of interacting pyramidal cells, whose activity episodically undergoes transient increases in spatial coherence. Gaussian i.i.d. random numbers are shaped by 1/f filters derived from stabilization at self-organized criticality [Freeman, 2004b], narrow temporal band pass filters from negative feedback, low pass spatial filters from volume conduction, and by spatial coherence from long-range positive feedback. The method suffices to replicate several features of background EEG and its changes with simulated state transitions, so it provides a tool that can be used to explore and optimize alternative methods for dealing with phase slip introduced by the Hilbert transform. Noteworthy are the steepened slope of 1/f PSD_T in sleep compared with the awake state (Fig. 1, E, F), which is easily simulated by changing α in equation (1) but not thereby explained, and the disappearance of the 1/f component from the PSD_X in the transition from sleep to awake, which reflects the enhanced long-range correlation that characterizes the awake and active state [Freeman, 2005; Freeman et al., 2005; Vitiello, 2001]. This change also appears in pre-ictal EEG [Freeman et al., 2005], so it might offer a clue to understanding the mechanisms of complex partial seizures and predicting their onsets. Other aspects of the method remain unexplored. The transition from high-voltage slow wave activity in sleep to low-voltage fast activity on arousal (Fig. 5, D) has not been explicitly simulated, nor have comparable EEG changes that precede seizure onset. The amplitude of the spatial ensemble average of the noise always increases with increasing spatial correlation, but other factors that might change amplitudes [Freeman, 1975] have not yet been explored with the method. Distance-dependent axonal propagation delays were not included, so there were no spatial phase gradients or phase cones in the simulated outputs. The spatial patterns of amplitude modulation (AM) of the carrier waves in beta and gamma frames have not been systematically modified, so there is as yet no basis for estimating the effect of changes in modulation depth on the classification of AM patterns.

A compelling experimental feature of the simulation is the demonstration of fluctuations in both the analytic amplitude squared, $A^2(t)$, and the pragmatic information index, $H_e(t)$, under sustained high levels of correlation (e.g., in frames lasting 2 s or more). A possible explanation is that these fluctuations are due to interference between the oscillations of the background activity and the correlated oscillations in the frames, owing to overlap in the pass bands of the temporal filters

used for generation and observation, because the variation was maximal when the generating and measuring pass bands were identical. The % correct classification from the rms amplitudes in frames of known locations (Fig. 7, A) was nearly the same as the % correct from use of $H_e(t)$ to locate the frames (B), so that uncertainty about the time location of frames may have had less impact on classification, if the distortion of amplitudes were due to interference. Perhaps that insensitivity to precise temporal location might explain why inclusion of the variance ratio, $R_e(t)$, among the criteria for frame location gave no improvement in classification rates. Alternatively the high variation might be due to departures from normality in the distributions of parameters as shown in Fig. 4, so that validation of this method of simulation will require review by experts in numerical analysis on digital platforms.

The fluctuations and the apparent foreshortening in frame durations of elevated $H_e(t)$ in simulated EEG imply that such interference also occurs in normal EEG, where it results from multiple coexisting domains of elevated correlation. If so, this interference phenomenon poses a major challenge for digital signal processing of spatial patterns of EEG in relation to behavior. How might the limitations imposed by band pass filtering be overcome? How do the targets of cortical transmission resolve mixed signals? These are experimental problems that will have to be solved in order to make effective use of the EEG in brain studies. This method of simulation provides a test bed with which to develop and evaluate new methods for digital signal processing.

The inverse relation of phase variability, $SD_X(t)$, and amplitude, $\underline{A}(t)$. is consistent with genesis of the time series, v(t), with filtered random numbers, because when A(t) approaches zero, phase is indeterminate and subject to errors of measurement and calculation, Spatially coherent noise generates CAPD with maximal differences at low power. This inverse relation was found with both Fourier and Hilbert techniques, as well as in the covariation of mean power, $\underline{A^2}(t)$, and synchrony, $R_e(t)$, so it was intrinsic to all three methods for the decomposition of filtered random numbers into time series for phase and amplitude. What distinguished the EEG from the simulation of background was its sequence of state transitions, which was simulated by imposing repeated frames in which the level of spatial coherence was increased, on the premise of intermittently increased dense and long-range cooperative synaptic interactions among pyramidal cells in the active state [Freeman, 2004b]. The ensemble average of a collection of independent time series obviously increases with increasing synchrony and with enhanced long-range correlation [Vitiello, 2001] and increased diameters of wave packets [Freeman, 2005]. This mechanism might account for the emergence of delta activity during slow wave sleep (Fig. 1, E, F), and for the relative overshadowing by lower voltage activity in higher frequency ranges on arousal (Fig. 5, D).

However, simulations of amplitude differed from the awake EEG in two respects: first that the onset of synchrony in EEG frames, as measured by $SD_X(t)$ and $R_e(t)$, preceded the increase in $\underline{A^2}(t)$ and were not simultaneous; and second that mean amplitude, $\underline{A}(t)$, might increase or decrease from the background level in successive frames of EEG, whereas in simulated frames the amplitude always increased (Fig. 5, A). In olfactory bulbar EEGs, furthermore, gamma bursts on inhalation of background air with no CSs tended to be larger than background levels, whereas gamma bursts on inhalation of air carrying CSs tended to be smaller, despite evidence from phase measurements of sustained synchrony. While it is well known that narrowing the pass

band of a temporal filter in electronic circuits decreases the amplitude of the oscillation about the center frequency of the output, this feature was not included in the simulation, because physiological documentation of changes in the pass band of neural feedback mechanisms during perception was inadequate. Therefore, the simulation poses for cellular physiologists [e.g., Traub et al., 1996; Whittington et al., 2000] the problem of analysis of the factors controlling changes in the intensity of dendritic currents that accompany the formation, transmission, and reception of AM patterns correlated with behavior.

The focus of this four-part study has been on measurement of AM patterns in order to classify those in the CS-CR interval with respect to the discriminated CSs that preceded them, because there is no alternative in validating spatiotemporal structures in EEG to behavioral correlation. The quality of validation is clearly given by the goodness of correct classification. By that standard the simple linear discriminant functions used in this study gave classifications well above chance levels but not sufficient for clinical and cognitive studies. Linear techniques have the advantage of simplicity and universality in early stages of exploring the statistical properties of EEG data sets. Advanced techniques such as ROC and nonlinear discriminant functions in the hands of experts can be expected to improve levels of classification substantially, provided that the underlying physiological processes have been understood and correctly modeled, and that the more complex methods have been tailored to the characteristics of the data.

References

Andersen P, Andersson SA. Physiological basis for the alpha rhythm. New York: Appleton, 1968.

Atmanspacher H, Scheingraber H. Pragmatic information and dynamical instabilities in a multimode continuous-wave dye laser. Can. J. Phys. 1990, 68: 728-737.

Barrie JM. Freeman WJ, Lenhart M. Modulation by discriminative training of spatial patterns of gamma EEG amplitude and phase in neocortex of rabbits. J. Neurophysiol. 1996, 76: 520-539.

Barrie JM, Holcman D, Freeman WJ. Statistical evaluation of clusters derived by nonlinear mapping of EEG spatial patterns. J Neurosci Meth 1999, 90: 87-95.

Basar E (1998) Brain Function and Oscillations. Berlin: Springer Verlag.

Braitenberg V, Schüz A. Anatomy of the Cortex: Statistics and Geometry. Berlin: Springer-Verlag, 1991.

Bressler SL and Kelso JAS. Cortical coordination dynamics and cognition. Trends Cog. Sci. 2001, 5: 26-36.

Bullock TH. The neuron doctrine and electrophysiology. Science 1969, 129: 997-1002.

Elul R. The genesis of the EEG. Int. Rev. Neurobiol. 1972, 15: 227-272.

Freeman WJ. Mass Action in the Nervous System. Academic Press, New York, 1975. Reprinted 2004: http://sulcus.berkeley.edu/MANSWWW/MANSWWW.html

Freeman WJ. Neurodynamics. An Exploration of Mesoscopic Brain Dynamics. London UK: Springer-Verlag, 2000.

Freeman WJ. A neurobiological theory of meaning in perception. Part 2. Spatial patterns of phase in gamma EEG from primary sensory cortices reveal the properties of mesoscopic wave packets. Int. J. Bifurc. Chaos 2003, 13: 2513-2535.

Freeman WJ. Origin, structure, and role of background EEG activity. Part 1. Analytic phase. Clin. Neurophysiol. 2004, 115: 2077-2088.

Freeman WJ. Origin, structure, and role of background EEG activity. Part 2. Analytic amplitude. Clin. Neurophysiol. 2004, 115: 2089-2107.

Freeman WJ.Origin, structure, and role of background EEG activity. Part 3. Neural frame classification. Clin. Neurophysiol. 2005, in press.

Freeman WJ, Barrie JM. Analysis of spatial patterns of phase in neocortical gamma EEGs in rabbit. J. Neurophysiol. 2000, 84: 1266-1278.

Freeman WJ, Burke BC and Holmes MD. Aperiodic phase re-setting in scalp EEG of beta-gamma oscillations by state transitions at alpha-theta rates. Hum. Brain Map. 2003, 19(4): 248-272.

Freeman WJ, Grajski KA. Relation of olfactory EEG to behavior: Factor analysis. Behav. Neurosci. 1987, 101: 766-777.

Freeman WJ, Holmes MD, West GA, Vanhatalo S. Dynamics of human neocortex that optimizes its stability and flexibility. Int. J. Intelligent Systems 2005, in press.

Freeman WJ, Rogers LJ. Fine temporal resolution of analytic phase reveals episodic synchronization by state transitions in gamma EEGs. J. Neurophysiol. 2002, 87: 937-945.

Freeman WJ, Rogers LJ, Holmes MD, Silbergeld DL. Spatial spectral analysis of human electrocorticograms including the alpha and gamma bands. J. Neurosci. Meth. 2000, 95: 111-121.

Fingelkurts AA and Fingelkurts AA. Making complexity simpler: Multivariability and metastability in the brain. Int. J. Neurosci. 2004, 114: 843-862.

Friston KJ. Transients, metastability and neural dynamics. Neuroimage 1997, 5: 164-171.

Friston KJ. The labile brain. I. Neuronal transients and nonlinear coupling. Phil Trans R Soc Lond B 2000, 355:215-236.

Haken, H. What can synergetics contribute to the understanding of brain functioning? In: Analysis of Neurophysiological Brain Functioning. Uhl, C, (ed.) Berlin: Springer-Verlag. pp. 7-40, 1999.

Hoppensteadt FC and Izhkevich EM. Thalamo-cortical interactions modeled by weakly connected oscillators: could the brain use FM radio principles? BioSystems 1998, 48: 85-94.

Houk J. Agents of the mind. Biol. Cybern. 2005, 92(6): in press.

Huang NE, Shen Z, Long SR, Wu MC, Shih HH, Zheng Q, Yen N-C, Tung CC, Liu HH. The empirical mode decomposition and the Hilbert spectrum for nonlinear and non-stationary time series analysis. Proc. R. Soc. Lond. 1998 454: 903-995.

Hwa RC and Ferree T. Scaling properties of fluctuations in the human electroencephalogram. Physical Rev. 2002, E 66: 021901.

Ingber L. Statistical mechanics of multiple scales of neocortical interactions. pp. 628-681 in: Nunez PL (ed.). Neocortical Dynamics and Human EEG Rhythms. New York: Oxford U.P., 1995.

König A. Interactive visualization and analysis of hierarchical neural projections for data mining. IEEE Trans. Neural Networks TNN 2000, 11: 615 - 624.

Kozma R, Freeman WJ. Chaotic resonance: Methods and applications for robust classification of noisy and variable patterns. Int. J. Bifurc. Chaos 2001, 10: 2307-2322.

Kozma R, Freeman WJ, Erdí P. The KIV model – nonlinear spatio-temporal dynamics of the primordial vertebrate forebrain. Neurocomputing 2003, 52: 819-826.

Kozma R, Puljic M, Balister P, Bollabás B, Freeman WJ. (2005) Phase transitions in the neuropercolation model of neural populations with mixed local and non-local interactions. Biol. Cybern. 2005, 92: 367-379.

Le Van Quyen M, Foucher J, Lachaux J-P, Rodriguez E, Lutz A, Martinerie J, Varela F. Comparison of Hilbert transform and wavelet methods for the analysis of neuronal synchrony. J. Neurosci. Meth. 2002, 111: 83-98.

Linkenkaer-Hansen K, Nikouline VM, Palva, JM, Iimoniemi RJ. Long-range temporal correlations and scaling behavior in human brain oscillations. J Neurosci 2001, 15: 1370-1377.

Miller LM, Schreiner CE. Stimulus-based state control in the thalamocortical system. .J Neurosci. 2000: 20:7011-7016.

Nunez PL. Electric Fields of the Brain: The Neurophysics of EEG. New York NY: Oxford University Press, 1981.

Panksepp, J. (1998) Affective Neuroscience. Oxford University Press.

Pikovsky A, Rosenblum M, Kurths J. Synchronization — A Universal Concept in Non-linear Sciences. Cambridge UK: Cambridge University Press, 2001.

Quiroga RQ, Kraskov A, Kreuz T, Grassberger P. Performance of different synchronization measures in real data: A case study on electroencephalographic signals. Physical Rev E 2002, 6504:U645-U658 - art. no. 041903.

Sammon JW. A nonlinear mapping for data structure analysis. IEEE Trans. Comput. 1969, C-18: 401-409.

Stam CJ, Breakspear M, van Cappellen van Walsum A-M, van Dijk BW. Nonlinear synchronization in EEG and whole-head recordings of healthy subjects. Hum Brain Mapp 2003, 19:63-78.

Traub RD, Whittington MA, Stanford IM, Jefferys JGR. A mechanism for generation of long-range synchronous fast oscillations in the cortex. Nature 1996, 383: 421-424.

Tsuda, I. Toward an interpretation of dynamics neural activity in terms of chaotic dynamical systems. Behav. Brain Sci. 2001, 24: 793-847.

Vitiello G. My Double Unveiled. Philadelphia: John Benjamins, 2001.

Wakeling JR. Adaptivity and 'Per learning'. Physica A 2004, 340: 766-773.

Whittington MA, Faulkner HJ, Doheny HC, Traub RD Neuronal fast oscillations as a target site for psychoactive drugs. Pharmacol. Therap. 2000, 86: 171-190.

Wilson HR, Cowan JD (1973) Excitatory and inhibitory interactions in localized populations of model neurons. Biophys. J. 1973, 12: 1-24.